Ultimate resolution for refractometric sensing with whispering gallery mode microcavities

J.W. Silverstone, S. McFarlane, C.P.K. Manchee, and A. Meldrum*

Department of Physics, University of Alberta, Edmonton, AB, T6G2G7, Canada
**ameldrum@ualberta.ca*

Abstract: Many proposed microfluidic biosensor designs are based on the measurement of the resonances of an optical microcavity. Fluorescence-based resonators tend to be simpler and more robust than setups that use evanescent coupling from tuneable laser to probe the cavity. In all sensor designs the detection limits depend on the wavelength resolution of the detection system, which is a limitation of fluorescence-based devices. In this work, we explore the ultimate resolution and detection limits of refractometric microcavity sensor structures. Because many periodic modes are collected simultaneously from fluorescent resonators, standard Fourier methods can be best suited for rapid and precise analysis of the resonance shifts. Simple numerical expressions to calculate the ultimate sensor resolution and detection limits were found, and the results compared to experiments in which the resonances of fluorescent-core microcapillaries responded to various sucrose concentrations in water.

OCIS codes: (070.2025) Discrete optical signal processing; (230.5750) Resonators; (140.3948) Microcavity devices; (070.4790) Spectrum analysis

References and links

1. K. E. Herold and A. Rasooly, eds., *Lab-on-a-Chip Technology: Fabrication and Microfluidics*. Caister Academic Press, 2009.
2. J. J. Amsden, P. Domachuk, A. Gopinath, and R. D. White, "L. D. Negro D. L Kaplan and F. G. Omenetto, "Biocompatible films: rapid nanoimprinting of silk fibroin films for biophotonic applications," Adv. Mater. (Deerfield Beach Fla.) **22**, 1–4 (2010).
3. A. H. Diercks, A. Ozinsky, C. L. Hansen, J. M. Spotts, D. J. Rodriguez, and A. Aderem, "A microfluidic device for multiplexed protein detection in nano-liter volumes," Anal. Biochem. **386**(1), 30–35 (2009).
4. D. Erickson, S. Mandal, A. H. J. Yang, and B. Cordovez, "Nanobiosensors: optofluidic, electrical and mechanical approaches to biomolecular detection at the nanoscale," Microfluid. Nanofluid. **4**(1-2), 33–52 (2008).
5. F. Vollmer and S. Arnold, "Whispering-gallery-mode biosensing: label-free detection down to single molecules," Nat. Methods **5**(7), 591–596 (2008).
6. A. M. Armani, R. P. Kulkarni, S. E. Fraser, R. C. Flagan, and K. J. Vahala, "Label-free, single-molecule detection with optical microcavities," Science **317**(5839), 783–787 (2007).
7. N. Jokerst, M. Royal, S. Palit, L. Luan, S. Dhar, and T. Tyler, "Chip scale integrated microresonator sensing systems," J. Biophotonics **2**(4), 212–226 (2009).
8. I. M. White, H. Oveys, and X. Fan, "Liquid-core optical ring-resonator sensors," Opt. Lett. **31**(9), 1319–1321 (2006).
9. I. M. White, H. Zhu, J. D. Suter, N. M. Hanumegowda, H. Oveys, M. Zourob, and X. Fan, "Refractometric sensors for lab-on-a-chip based on optical ring resonators," IEEE Sens. J. **7**(1), 28–35 (2007).
10. V. Zamora, A. Díez, M. V. Andrés, and B. Gimeno, "Refractometric sensor based on whispering-gallery modes of thin capillarie," Opt. Express **15**(19), 12011–12016 (2007).
11. S. Arnold, M. Khoshsima, I. Teraoka, S. Holler, and F. Vollmer, "Shift of whispering-gallery modes in microspheres by protein adsorption," Opt. Lett. **28**(4), 272–274 (2003).
12. A. Francois and M. Himmelhaus, "Optical biosensor based on whispering gallery mode excitations in clusters of microparticles," Appl. Phys. Lett. **92**(14), 141107 (2008).
13. F. Vollmer, S. Arnold, and D. Keng, "Single virus detection from the reactive shift of a whispering-gallery mode," Proc. Natl. Acad. Sci. U.S.A. **105**(52), 20701–20704 (2008).
14. P. Bianucci, J. R. Rodríguez, C. M. Clements, J. G. C. Veinot, and A. Meldrum, "Silicon nanocrystal luminescence coupled to whispering gallery modes in optical fibers," J. Appl. Phys. **105**(2), 023108 (2009).

#161306 - $15.00 USD Received 11 Jan 2012; revised 27 Feb 2012; accepted 4 Mar 2012; published 26 Mar 2012

15. I. M. White and X. Fan, "On the performance quantification of resonant refractive index sensors," Opt. Express **16**(2), 1020–1028 (2008).
16. H. T. Beier, G. L. Coté, and K. E. Meissner, "Modeling whispering gallery modes in quantum dot embedded polystyrene microspheres," J. Opt. Soc. Am. B **27**(3), 536–543 (2010).
17. S. Pang, R. E. Beckham, and K. E. Meissner, "Quantum dot-embedded microspheres for remote refractive index sensing," Appl. Phys. Lett. **92**(22), 221108 (2008).
18. D. E. Gómez, I. Pastoriza-Santos, and P. Mulvaney, "Tunable whispering gallery mode emission from quantum-dot-doped microspheres," Small **1**(2), 238–241 (2005).
19. A. Salinas-Castillo, M. Camprubí-Robles, and R. Mallavia, "Synthesis of a new fluorescent conjugated polymer microsphere for chemical sensing in aqueous media," Chem. Commun. (Camb.) **46**(8), 1263–1265 (2010).
20. A. Beltaos and A. Meldrum, "Whispering gallery modes in silicon-nanocrystal-coated silica microspheres," J. Lumin. **126**(2), 607–613 (2007).
21. E. Nuhiji and P. Mulvaney, "Detection of unlabeled oligonucleotide targets using whispering gallery modes in single, fluorescent microspheres," Small **3**(8), 1408–1414 (2007).
22. A. Weller, F. C. Liu, R. Dahint, and M. Himmelhaus, "Whispering gallery mode biosensors in the low-Q limit," Appl. Phys. B **90**(3-4), 561–567 (2008).
23. M. Charlebois, A. Paquet, L. S. Verret, K. Boissinot, M. Boissinot, M. G. Bergeron, and C. N. Allen, "Toward automatic label-free whispering gallery modes biodetection with a quantum dot-coated microsphere population," Nanoscale Res. Lett. **5**(3), 524–532 (2010).
24. A. G. Piersol, "Time delay estimation using phase data," IEEE Trans. Acoust. Speech Signal Process. **29**(3), 471–477 (1981).
25. W. C. Karl and H. H. Pien, "High-resolution biosensor spectral peak shift estimation," IEEE Trans. Signal Process. **53**(12), 4631–4639 (2005).
26. M. Suematsu and M. Takeda, "Wavelength-shift interferometry for distance measurements using the Fourier transform technique for fringe analysis," Appl. Opt. **30**(28), 4046–4055 (1991).
27. F. Bruyneel, H. De Smet, J. Vanfleteren, and A. Van Calster, "Method for measuring the cell gap in liquid-crystal displays," Opt. Eng. **40**(2), 259–267 (2001).
28. C. M. Hessel, M. A. Summers, A. Meldrum, M. Malac, and J. G. C. Veinot, "Direct patterning, conformal coating, and erbium doping of luminescent nc-Si/SiO2 thin films from solution processable hydrogen silsesquioxane," Adv. Mater. (Deerfield Beach Fla.) **19**(21), 3513–3516 (2007).
29. C. P. K. Manchee, V. Zamora, J. W. Silverstone, J. G. C. Veinot, and A. Meldrum, "Refractometric sensing with fluorescent-core microcapillaries," Opt. Express **19**(22), 21540–21551 (2011).
30. A. W. Poon, R. K. Chang, and J. A. Lock, "Spiral morphology-dependent resonances in an optical fiber: effects of fiber tilt and focused Gaussian beam illumination," Opt. Lett. **23**(14), 1105–1107 (1998).
31. A. L. Stancik and E. B. Brauns, "A simple asymmetric lineshape for fitting infrared absorption spectra," Vib. Spectrosc. **47**(1), 66–69 (2008).
32. N. R. Lomb, "Least-squares frequency analysis of unequally spaced data," Astrophys. Space Sci. **39**(2), 447–462 (1976).
33. Santa Barbara Instruments Group, *http://www.sbig.com/site/*, Pers. Comm.
34. V. Zamora, A. Diez, M. V. Andres, and B. V. Gimeno, "Cylindrical optical microcavities: basic properties and sensor applications," Photonics and Nanostructures – Fundamentals and Applications **9**, 149–158 (2011); also V. Zamora and A. Meldrum, unpublished results.

Introduction

The development of inexpensive Lab-on-a-Chip (LoC) microfluidic sensors could lead to new proteomic and pharmaceutical detection and analysis methods [1,2]. Such systems should be label-free, robust, inexpensive, and parallelizable [3], and they should handle a small analyte volume [3]. The analyses should be both rapid and sensitive to low concentrations of the target compound [4]. Microscale optical ring resonators could potentially meet many of these requirements. In ring resonators, light circulates by total internal reflection around the resonator periphery, causing the development of resonances known as the whispering gallery modes (WGMs). The evanescent field of the WGMs samples the medium adjacent to the resonator, shifting the resonant frequency. By functionalizing the surface for binding to specific analytes, WGM biosensors can be fabricated that meet many of the above requirements for LoC sensing technologies [5].

Lithographically defined microdisks [6,7], liquid-core optical ring resonators (LCORRs) [8–10] microspheres [11–13] and even optical fibers [14] can be employed as WGM-type refractometric sensors. In many of these structures, light from a tuneable laser is evanescently coupled to the resonator through a waveguide or a tapered fiber. The WGM central wavelength and linewidth are measured as the laser is scanned across one of the resonances,

#161306 - $15.00 USD Received 11 Jan 2012; revised 27 Feb 2012; accepted 4 Mar 2012; published 26 Mar 2012

and shifts due to changes in the local fluid index are measured. Two figures of merit for such devices are the refractometric sensitivity, $S = d\lambda/dn$, which describes the magnitude of the wavelength shift due to changes in the fluid index of refraction, and the refractometric detection limit Δn_{min}. The sensitivity is an inherent property of the device; however, the detection limit – the more important figure in practice – is given by $\Delta n_{min} = \delta\lambda/S$ where $\delta\lambda$ is the minimum detectable wavelength shift in the measurement system, *i.e.*, the resolution.

The system resolution, $\delta\lambda$, is a thus an important parameter in refractometric and biosensor WGM devices. It has previously been defined as three standard deviations (3σ) of the estimated mode peak position [15]:

$$\delta\lambda = 3\sigma = 3\sqrt{\sigma_{peak}^2 + \sigma_{temp}^2 + \sigma_{res}^2}. \quad (1)$$

In Eq. (1), σ_{res} is the measurement system's wavelength resolution, σ_{temp} is the WGM peak deviation due to temperature instability (*i.e.*, uncertainties in the resonance positions due to thermo-optic and thermal expansion effects), and σ_{peak} is the uncertainty arising from the spectral noise. The second equality in Eq. (1) holds when the independent contributions can be obtained without sampling-related limitations in the data analysis. Numerical results obtained by statistically analyzing the frequency of the maximum point in the mode for heavily oversampled simulated data with white noise indicated that [15]:

$$\sigma_{peak} = \frac{\Delta\lambda_{peak}}{4.5 \cdot SNR^{0.25}}. \quad (2)$$

In Eq. (2), the SNR is the signal-to-noise ratio in linear units and $\Delta\lambda_{peak}$ is the WGM peak width in wavelength. For brevity, we will refer to this method – that is, finding the mode center by picking the maximum point – as "peak picking" in the text to follow. This is, obviously, the simplest way to identify the peak position. For values of σ_{res}, σ_{temp}, and σ_{peak} characteristic of ring resonators coupled evanescently to a tuneable laser, one arrives at typical detection limits of ~10^{-6} refractive index units (RIU) [15].

Incorporating a fluorescent dye or quantum dots into the resonator structure permits operation in the fluorescence mode. In this mode, the WGMs appear as peaks in a fluorescence spectrum rather than as dips in a laser transmission spectrum. Compared with evanescent coupling, fluorescence-based systems are attractive because (i) one does not need to fabricate tapered fibers or waveguides; (ii) delicate nanopositioning equipment for evanescent coupling is not required; (iii) the tuneable laser, which is an expensive investment, can be replaced with a diode laser or LED to excite the fluorescence; and, (iv) the devices can be easily fabricated and are mechanically robust. With respect to signal processing, an additional advantage of fluorescence devices is that many periodic WGMs are collected simultaneously over a range of frequencies.

The main drawbacks with fluorescence-based systems are associated with the use of a grating spectrometer to analyze the WGMs. Whereas, for a tuneable laser system σ_{res} can be less than 1 pm, our spectrometer has a manufacturer-quoted instrument resolution, R, of 0.24 nm and a sampling pitch, P, of 0.1 nm/pixel. Thus, a blind application of Eq. (1) would suggest a detection limit (assuming $\sigma_{res} = P$ with all other uncertainties being insignificant) of $\delta\lambda$ = 0.3 nm – around 3 orders of magnitude worse than for a tuneable laser evanescently coupled to a microcavity. A second problem with fluorescence-based WGM sensor systems is the much lower signal intensity. This leads to a low SNR and a corresponding difficulty in ascertaining the peak position, unless the collection time is long. This problem can limit "live" data collection during real-time changes in analyte concentration. Thus, fluorescence-based WGM refractometric sensors, which have otherwise several attractive properties, evidently suffer from low resolution, poor sampling of the signal, and long collection times.

#161306 - $15.00 USD Received 11 Jan 2012; revised 27 Feb 2012; accepted 4 Mar 2012; published 26 Mar 2012

In this paper, the resolution and detection limits for WGM sensors will be examined more closely. Although specifically motivated by fluorescence WGM systems, the conclusions will hold for the evanescent type also. Numerical models that give the system resolution under a variety of experimental conditions will be obtained, and the results compared with a "real life" experimental case in which the WGMs have non-Lorentzian peak shapes due to mode overlap.

Numerical methods

Previous investigations using fluorescent WGMs have often been conducted with commercial microspheres containing a fluorescent dye or quantum dots [16–20]. The method used to determine the WGM peak location is not always reported [21]; however, usually one of four methods are used to determine the WGM spectral position: (i) visual estimation; (ii) finding the maximum point in the mode (peak picking); (iii) parametric waveform analysis (*i.e.*, curve fitting) with an appropriate function over a single mode [14,22]; or, (iv) performing autocorrelations to estimate $\Delta\lambda$ rather than finding λ_{peak} [12,23]. In every method uncertainty arises from spectral noise, from the varying background, and sometimes from overlapping modes.

The periodic WGM fluorescence spectrum readily lends itself to modeling with standard frequency-domain signal processing methods. Changing the concentration of the solution leads to a shift-invariant phase delay of the entire waveform, at least over a narrow range of refractive index. If the refractive index variation is large, the waveforms are not strictly shift invariant. For example: the Q-factor is affected by the refractive index contrast and absorption in concentrated solutions, and the sensitivity can vary over the range of WGM wavelengths collected. However, for high-resolution measurements, the refractive index change should be as small as possible; thus we can safely assume a "pure delay" (*i.e.*, waveform shift invariance). More advanced methods could be used in cases where a pure delay cannot be safely assumed [24].

In contrast, evanescent measurements are usually limited to a narrow range of wavelengths, sometimes less than one FSR. In such cases the WGM periodicity is not observed; however, the waveform can be fit numerically if one has a model that represents the data. Ideally, a WGM should be characterized by a Lorentzian lineshape; however, in several examples (such as the one shown in the experimental results described below) mode overlaps make the selection of an appropriate model considerably more difficult and can degrade the ultimate device resolution.

Here, two methods will be used for extraction of the WGM peak positions: parametric waveform analysis (henceforth referred to as curve fitting, or "CF") over a single peak, and the discrete Fourier transform (DFT) followed by a shift-invariant linear phase analysis over the whole spectrum. Both methods should, obviously, be better than "peak picking", but the ultimate practicable WGM wavelength shift resolution with either method is open to comparison. Frequency domain methods have been widely applied to biosensing [25], wavelength shift interferometry [26], optical thickness measurements [27], and many other fields, but they have not yet been used in WGM refractometric sensors.

To explore how the detection limit depends on the SNR and quality factor of the WGMs, test spectra were generated as a set of equally-spaced Lorentzians with Gaussian noise producing SNRs (= $A_{signal}/A_{noise})^2$ from 1 to 10^5 (Fig. 1(a)). The Lorentzian lineshape is typical for many types of microcavities (although not exactly for our FCM structures, as will be discussed further, below. To estimate the detection limits, a large number of these spectra with the same underlying train of Lorentzians was calculated, similar to the method described in Ref [15]. The process was repeated over a large parameter space with SNR from 1 to 10^5, mode peak widths from 0.05 to 1.6 THz (Q from ~7500 to 230 at λ = 800 nm), and a sampling pitch from 50 GHz to 1.6 THz (0.1 nm to 3.4 nm at λ = 800 nm). The resolution $\delta\lambda$ was then obtained using either CF or DFT methods, as 3σ of the standard deviation about the expected zero phase shift.

#161306 - $15.00 USD Received 11 Jan 2012; revised 27 Feb 2012; accepted 4 Mar 2012; published 26 Mar 2012

Curve fitting

In the curve fitting procedure, a single peak was chosen from the middle of the simulated spectra in Fig. 1(a), and was fit with a Lorentzian function. The standard-deviation of the resulting CF peak positions over many spectra (with mean shift equal to zero) was then tripled to obtain the 3σ resolution, $\delta\lambda$. The results are shown in Fig. 1(b), for an experimental sampling pitch of 47 GHz. The values obtained represent the 3σ deviation of the uncertainty in the peak position, as a function of the SNR and WGM peak width. A nonlinear power-law regression was performed ($r^2 = 0.97$) to develop the model shown by the colored plane in Fig. 1(b), given by:

$$\Delta\lambda_{\min}(3\sigma) = \frac{2.2\text{x}10^{-20} \cdot \Delta f_{peak}^{0.29} \cdot P^{0.65}}{SNR^{0.51}} \text{ meters.} \qquad (3)$$

Here, Δf_{peak} and the pitch, P are in units of Hz, and the SNR is in linear units. In Fig. 1(b), different sampling pitches would result in different solution surfaces.

Equation (3) shows that for a reasonably high SNR and a Q-factor around 1000, the curve fitting resolution is in the range of picometers for a fluorescence-based system with a pitch of 0.1 nm. However, the analysis encounters limits at the extremes of the Q factor. For example, at high Q (or, equivalently, for a large pitch) the sampling rate approaches the Nyquist rate. For typical spectrometer systems, this happens at Q factors around 10^4. In the opposite case, that of very low Q, curve fitting is hampered by overlaps from adjacent angular mode orders as $\Delta f_{peak} \rightarrow$ FSR.

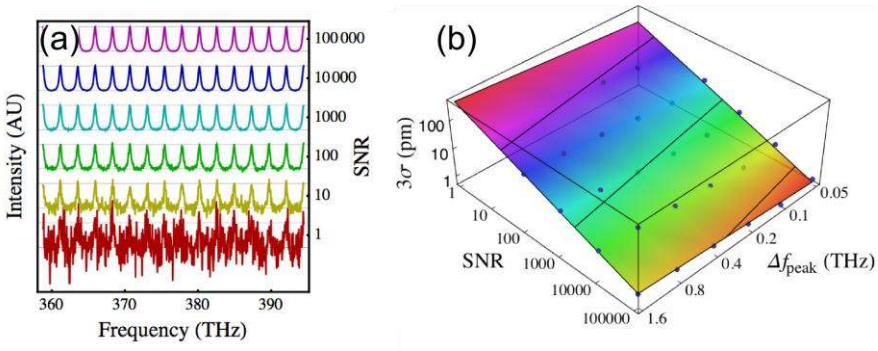

Fig. 1. (a) a set of simulated spectra with different SNRs, offset for clarity. (b) the 3σ resolution (vertical axis) as a function of the SNR and the WGM peak width, Δf_{peak}, obtained by least squares Lorentzian curve fitting to one of the modes in each spectrum. The pitch was 47 GHz. The colored plane represents the best fit solution for the system (given by Eq. (3)), giving an r^2 value of 0.97.

Fourier analysis

Alternatively, one can obtain the Fourier transform of the whole WGM spectrum to find the waveform phase shift. Some care is needed in the terminology: the term *frequency* spectrum will be used to describe the initial data (since the units are Hz) and *Fourier* spectrum to describe the transformed result. The k^{th} Fourier component represents periodicity in the data with "period" (in units of Hz) equal to $(f_{max} - f_{min})/k$. In this k^{th} component, an uncertainty or a shift of $\Delta\varphi$ represents a shift in real frequency units of $\Delta f = \Delta\varphi(f_{max} - f_{min})/2\pi k$. The wavelength shift $\Delta\lambda$ can be calculated by assuming that the real frequency of each datum is much larger than the frequency interval described by the whole spectrum, giving $\Delta\lambda = -4\Delta f\, c/(f_{max} + f_{min})^2$, where c is the speed of light in vacuum.

#161306 - $15.00 USD Received 11 Jan 2012; revised 27 Feb 2012; accepted 4 Mar 2012; published 26 Mar 2012

For a strongly periodic waveform such as a WGM frequency spectrum, the main feature of the Fourier power (or magnitude) spectrum corresponds to the FSR (Fig. 2(a)), with its harmonics describing the remainder of the periodic variation. However, all components of the Fourier spectrum contain information about the phase construction of the original data, and can be useful in determining the shift between two waveforms.

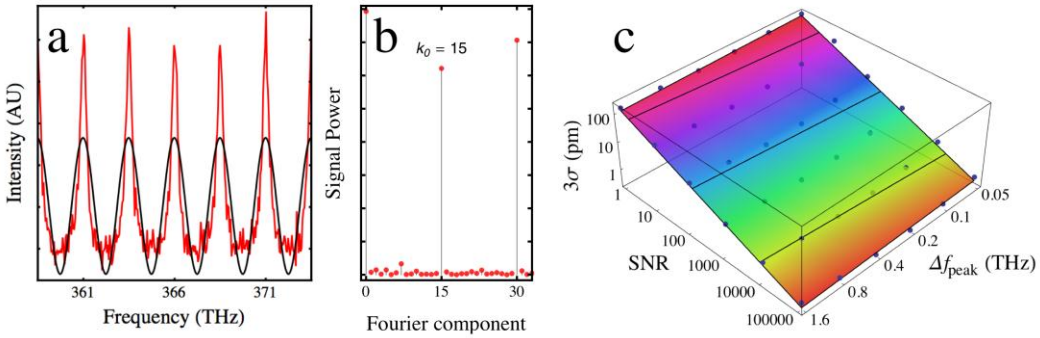

Fig. 2. (a) the dominant sinusoidal component of the DFT spectrum (black), corresponding to the FSR of the resonances, along with the original Lorentzian WGMs (red). (b) the power spectrum (squared magnitude of the Fourier components) of the spectral waveform. The 15th component clearly dominates, reflecting the strongly periodic nature of the simulated WGM spectrum; (c) the 3σ resolution for the DFT method, as a function of the SNR and the WGM peak width. As in Fig. 2, the colored surface is the linear least squares best fit solution (given by Eq. (4)) to the numerical results for P = 47 GHz, showing in this case r^2 = 0.99.

Assuming that the only change is a pure-shift (the waveform exactly maintains its shape, but translates in frequency), one can perform a weighted linear regression on this phase-difference spectrum. The regression is of the form $a \cdot k$, where the frequency shift, Δf, is related to the coefficient a according to $\Delta f = -a(f_{max} - f_{min})/2\pi$. The regression of the phase components is weighted by the corresponding power components in order to suppress phase noise in the less important frequencies present in the data. Here, a simple rectangular bandpass filter with (arbitrary) cutoffs at $k = 12$ and $k = 72$ was used in order to suppress the effect of shifts in both the low-frequency spectral background and the high-frequency noise.

By repeating each phase analysis 50 times with a different random noise, $\delta\lambda$ was obtained for each combination of parameters as the 3σ deviation in the calculated shifts. The main results are summarized in Fig. 2(c). Compared to the curve fitting map (Fig. 1(b)), the surface is sloped oppositely with respect to Δf_{peak}; *i.e.*, in this case, lower-Q WGMs give generally better detection limits. The numerical results were well described (r^2 = 0.99) by the following expression:

$$\Delta\lambda_{\min} = \frac{1.75x10^{-14}\,P^{0.50}}{\Delta f_{peak}^{0.12} \cdot SNR^{0.52}} \text{ meters.} \qquad (4)$$

The unit of each parameter is the same as in Eq. (3), previously. Over the parameter range that was studied, the detection limit scaled as the square root of the spectrometer pitch and approximately as the inverse square root of the SNR.

The analysis in Ref. [15] gives a resolution of 3.1 pm for a WGM with $Q = 10^4$, λ_{peak} = 1550 nm, SNR = 10^6, and P = 1 pm (where the authors used 0.29 pm in their calculation, assuming one standard deviation of a 1-pm-wide Gaussian distribution); whereas for curve fitting one obtains $\delta\lambda$ = 3.4 fm. The frequency-domain method (Eq. (4)) gives $\delta\lambda$ = 7.4 fm for these conditions. In this case, the transform performs worse than the curve-fitting method. Alternatively, taking a WGM system more similar to our fluorescent microcapillary devices (Q = 300, λ_{peak} = 800 nm, P = 47 GHz, SNR = 100), Eqs. (1) and (2) yield $\delta\lambda$ = 341 pm. Curve

#161306 - $15.00 USD Received 11 Jan 2012; revised 27 Feb 2012; accepted 4 Mar 2012; published 26 Mar 2012

fitting (Eq. (3)) gives $\delta\lambda$ = 58 pm, whereas the DFT provides a resolution of $\delta\lambda$ = 11 pm. In a typical fluorescence WGM system in which the mode periodicity is observable, the best resolution can thus be achieved by a simple frequency-domain analysis. These results are summarized in Table 1.

Table 1. Comparison of the ultimate resolution for fluorescence and evanescent WGMs.

Parameter	Fluorescent WGM		Evanescent WGM	
	Eq. (2)	Eq. (4)	Eq. (2)	Eq. (3)
Q	300	300	10^4	10^4
P	0.1 nm	47 GHz	1 pm	125 MHz
λ_{peak}	800 nm	800 nm	1550 nm	1550 nm
SNR	100	100	10^6	10^6
$\Delta\lambda_{min}$ (3σ)	341 pm	11 pm	3.1 pm	3.4 fm

There are several interesting results for values typical of a fluorescence WGM system. First, the resolution obtained from the DFT can be good, even for a low SNR. This suggests that the long collection times often used for fluorescence WGM analyses may not be strictly necessary, depending on the required detection limit. The effect of the data collection time will be confirmed experimentally below; FCM collection times as short as 1 second (reasonable even compared to evanescently-coupled setups using a tuneable laser) will produce a resolution at least similar to the spectrometer pitch when the spectral shifts are extracted from the DFT.

Experimental

The experimental test samples consisted of silica microcapillaries (inner diameter = 25 μm) with a layer of silicon quantum dots (QDs) coated on the channel surface (Fig. 3). The film, with an effective index of ~1.67 and a thickness of ~0.5 μm, supports fluorescence WGMs whose electric field extends slightly into the capillary channel. When excited with a blue LED or laser, the QDs emit a broad luminescence band centered near a wavelength of 800 nm. These fluorescent-core microcavities (FCMs) are similar to LCORRs [15], except that the resonances are measured in the fluorescence mode; also the device is mechanically robust and does not require pre-thinning treatments.

We previously presented the method for fabricating these fluorescent core microcavities [28,29]. Here, the 488 nm line of an Ar^+ laser was used to excite the QD fluorescence in free space above a microscope objective lens, using an incident laser power of ~40 mW. Solutions consisting of sucrose dissolved in water were pumped through the capillary channel while the fluorescence spectrum was monitored. For each sucrose solution, the FCM was first cleaned with deionized water, the solution was pumped in, and the fluorescence spectrum was collected. In each subsequent measurement the target Δn was 0.0012 RIU. Given an estimated sensitivity of ~10 nm/RIU for these devices based on electromagnetic simulations of the structure, this corresponds to an approximate target wavelength shift of ~12 pm; *i.e.*, 20 times smaller than the quoted resolution of the spectrometer and almost 9 times smaller than the pitch. A second set of data was collected, in which the collection time was varied in order to determine the effect of different SNRs on the spectral shift measurements. Errors were estimated by repeating the measurements for a single sucrose solution. Uncertainty in the fluid refractive index was obtained by accounting for the various systematic and random errors in the dilution and concentration-to-index conversion processes that were carried out.

#161306 - $15.00 USD Received 11 Jan 2012; revised 27 Feb 2012; accepted 4 Mar 2012; published 26 Mar 2012

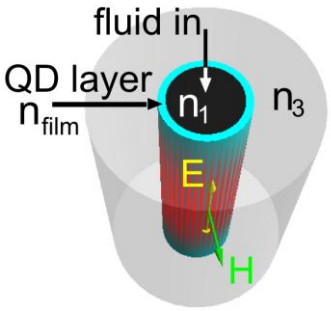

Fig. 3. Diagram of an FCM consisting of a capillary with an high-index fluorescent QD layer (cyan) coated on the channel surface. The field directions for the TE polarization are shown in yellow and green.

Analysis of experimental data

The fluorescent microcapillary WGMs were asymmetric with short-wavelength tails (Fig. 4). The high-frequency asymmetric tails are most likely due to cylindrical spiralling modes. This identification is consistent with several observations: (i) these mode asymmetries were not observed in similarly-sized microspheres prepared and coated with the same methods; (ii) the mode tails maintained a constant spectral relationship with the main peaks over the full range of n_1, thus ruling out the possibility of higher-order radial modes (which have higher refractometric sensitivity); (iii) spiralling modes are naturally on the high-frequency side of the main peaks [30], as observed here; and, (iv) a polarizer was used to collect only the modes whose electric field was parallel to the FCM axis (TE modes), thus ruling out overlapping modes of different polarization.

Here, we have the common problem associated with waveform analysis: the selection of a model that describes the data correctly. Unfortunately, there is no known function that describes a set of overlapping spiralling WGMs. The spiralling modes present a continuum of Lorentzians shifted to shorter wavelengths by an amount $\pi r\theta^2/(n\lambda)$ for small spiralling angle θ [30], but there are no expressions to calculate the angular dependence of the spiral mode intensity, $I(\theta)$. Thus, one is faced with a curve shape for which there is no analytical expression: it is comprised of a main Lorentzian on which is superimposed a continuum of shorter wavelength Lorentzians whose amplitude decreases with θ.

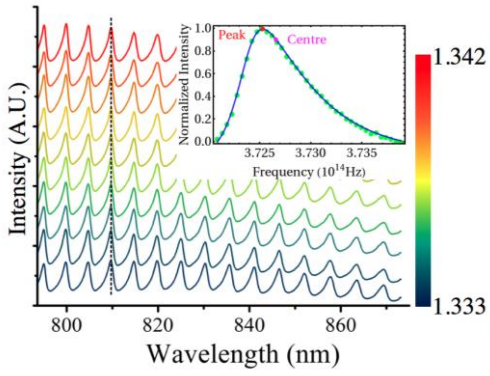

Fig. 4. The main panel shows the WGM spectrum for each 0.0012-RIU step in the solution refractive index, in wavelength units. The vertical dashed line is a guide to the eye, showing that the shift of a single mode is difficult to observe. The data are offset for clarity. The inset shows one of the peaks (converted to frequency units) with the skewed Lorentzian fit, showing the location of the peak and centre (f_0) frequencies.

#161306 - $15.00 USD Received 11 Jan 2012; revised 27 Feb 2012; accepted 4 Mar 2012; published 26 Mar 2012

We searched for a candidate function that can closely describe the observed asymmetric mode shapes. One such possibility is the skewed Lorentzian originally defined for infrared molecular transitions [31], given by

$$P(f) = \frac{2A}{\pi\gamma(f)} \Big/ \left[1 + 4\left(\frac{f - f_0}{\gamma(f)} \right)^2 \right]. \tag{5}$$

Here, f_0 is the central frequency, A is a normalizing factor, and the peak width γ describes the frequency-dependence of the skewing:

$$\gamma(f) = \frac{(1+B)\gamma_0}{1 + B \cdot e^{a(f-f_0)}}. \tag{6}$$

In Eq. (6), the exponential term describes a sigmoidal variation in the peak width centered around the frequency f_0, where a is a skew parameter that controls how the Lorentzian width varies around the central frequency. We introduce an additional parameter, B, that causes an asymmetry in the variation of the peak width. When $B = 0$ or $a = 0$, $P(f)$ is a pure Lorentzian of width γ_0. This model fit well to simulated spectra consisting of overlapping Lorentzians with essentially any $I(\theta)$. The inset to Fig. 4 shows that Eqs. (5) and (6), with a negative a and fractional B parameter, provide a good model for the experimental data as well, although there are noticeable deviations at the extrema – possibly due to overlap with adjacent mode orders.

The frequency-domain shift analysis method presented its own practical complication, as well. Conversion of the wavelength spectrum into frequency is necessary to ensure that the WGMs are regularly spaced and shift uniformly with small changes in analyte index, but directly converting the wavelength data to frequency leads to a non-uniform sampling pitch. This was handled by uniformly sampling a linear interpolation of the wavelength data. More advanced methods such as least squares frequency analysis [32] do exist for dealing with non-uniform sampling but these were not employed here.

The experimental WGM peak shift obtained by the peak-picking, curve fitting, and DFT methods are shown in Fig. 5. Although the correlation was poor for the peak-picking method and the error in the slope correspondingly high, even this crude technique appears sufficient to extract meaningful information on the sensitivity, given good sampling and SNR. Curve fitting with Eqs. (5) and (6) also demonstrated the expected spectral redshift with increasing refractive index over the narrow range investigated (Fig. 5(b)). The frequency-domain method showed a better correlation than the curve fitting (Fig. 5(c)), in agreement with the numerical simulations which predict a higher resolution for the DFT under these experimental conditions. The sensitivities for all three methods agree within error.

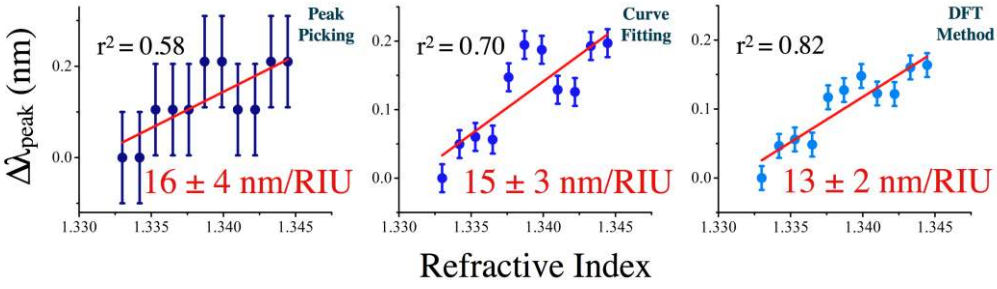

Fig. 5. Wavelength shifts for the spectra in Fig. 4 (SNR = 3×10^5) obtained using different methods. Left: peak picking; Middle: curve fitting; Right: weighted fit of the Fourier phase components. The error bars are one standard deviation from 10 repetitions of a single-index measurement and shift analysis. The first two methods used a peak centered at 382 THz.

The effect of increasing noise on the sensitivity was obtained for both curve fitting and DFT peak shift methods. Example spectra are shown in Fig. 6, for four different collection

#161306 - $15.00 USD Received 11 Jan 2012; revised 27 Feb 2012; accepted 4 Mar 2012; published 26 Mar 2012

times that gave SNRs ranging from 3 x 10^5 down to < 1. The solution refractive index was increased in 0.0012 RIU steps, as before, in order to extract the experimental sensitivity and resolution, $\delta\lambda$, as a function of the SNR (Table 2). For a low SNR = 6, corresponding to a 1-second collection time in our setup, curve fitting and especially the Fourier analysis can still deduce a good correlation between the wavelength shift and the refractive index change (Fig. 7). For a terrible SNR of ~0.5 (red curve in Fig. 6, corresponding to a 100-ms collection time), the WGM shifts were still resolvable by the frequency-domain method, and gave a slope in good agreement with those obtained from the longer collection times.

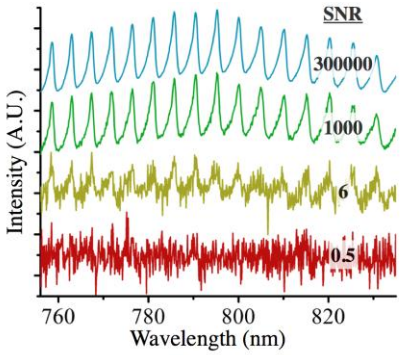

Fig. 6. The same spectrum taken with four different collection times (240s, 10s, 1s, and 0.1s) with the corresponding SNR. All spectra were taken with water inside the capillary channel.

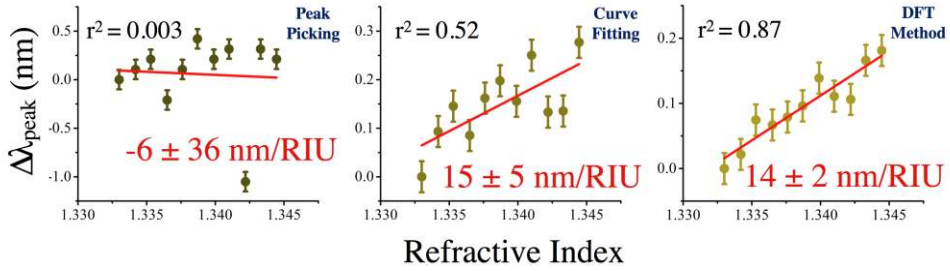

Fig. 7. WGM peak shifts as a function of RI, for an SNR = 6. A reasonable correlation can still be extracted from the DFT method; whereas for peak picking the spectral shift information is lost. In this case, for technical reasons the data was collected only once. The errors in the CF and DFT method were drawn from their (assumed) 3σ normal distribution about the linear model, and for the peak picking method, the error was assumed the same as in Fig. 5a where the spectral data collection was repeated.

An analysis of the residuals permits one to extract an estimate of $\delta\lambda$ (the experimental resolution for each analysis method), assuming that the residuals are normally distributed about the mean. The measured results are tabulated and compared against the predictions of the numerical models in Table 2, for an observed WGM peak with f_{peak} = 382 THz, Δf_{peak} = 1 THz, and an experimental sampling rate of P = 47 GHz (~0.1 nm). Generally, the trends are in agreement with the numerical predictions but the absolute experimental results are worse than those predicted numerically, particularly for the high SNR cases. Consistent with the numerical results, the frequency-domain method gives a better resolution than curve fitting for all the SNR values collected.

#161306 - $15.00 USD Received 11 Jan 2012; revised 27 Feb 2012; accepted 4 Mar 2012; published 26 Mar 2012

Table 2. Experimental and numerical results for a wide range of experimental SNRs. The subscripts *n* and *e* refer to numerical and experimental values, respectively.

SNR	Curve fitting			Fourier		
	S ***(nm/RIU)***	$3\sigma_e$ ***(pm)***	$3\sigma_n$ ***(pm)***	***S*** ***(nm/RIU)***	$3\sigma_e$ ***(pm)***	$3\sigma_n$ ***(pm)***
0.5	–6 ± 36	na	818	12 ± 4	149	149
6	15 ± 5	153	230	14 ± 2	57	58
1000	14 ± 2	79	17	12 ± 2	59	4
$3x10^5$	15 ± 3	110	0.9	13 ± 2	65	0.2

For the highest SNR studied, one would expect a much better resolution than that observed experimentally. While we cannot isolate the source of this discrepancy, the shifts may be contaminated by other random and systematic errors, such as: (i) the non-Lorentzian peak shapes compounded by mode overlap from adjacent angular modes; (ii) small motions of the capillary on the spectrometer slit, leading to deviations associated with the position of the spectrum on the CCD array, as communicated to us by the spectrometer manufacturer [33]; (iii) the spectral image focus, which was found to vary slightly from measurement to measurement; (iv) temperature variations, and (v) even over such small variations in the sucrose concentrations, the assumption of shift-invariance may not be strictly valid.

Discussion

The results show that the technique used to extract the peak shifts is an important consideration in the ultimate sensitivity and detection limit for WGM devices, and the optimal method will depend on the experimental and sampling conditions. Although the methods used are simple from a signal processing point of view, as applied to WGM-based refractometric sensors they may help to pave the way to improvements in both in the detection limits and analysis time for fluorescence-based WGM systems. In the case of fluorescence WGMs, under optimal conditions the resolution limit is almost two orders of magnitude smaller than the spectrometer resolution and pitch, while experimentally for a non-ideal mode structure we obtained an order-of-magnitude improvement over the pitch.

The FCM structures we studied here, although attractive from a microfluidic standpoint, have unfortunately a fairly low sensitivity in this refractive index range and suffer from WGM peak overlaps associated with spiralling cylindrical modes. Higher sensitivity in fluorescence WGMs can be obtained in at least two ways: (i) using QD-coated microspheres instead of capillaries, for which values as high as 160 nm/RIU can be achieved [17], and which feature a Lorentzian mode structure; and (ii) using high refractive-index fluids for which fluorescent capillaries demonstrate sensitivities of ~300 nm/RIU for the second order radial modes [34]. Smaller microspheres (which by nature have greater sensitivities) also demonstrate an attractive mode structure for data analysis, without observable peak overlap [22].

The SNR for a 1-second exposure time is ~6. However, a simple Fourier analysis was nevertheless able to provide 3σ experimental uncertainties as low as 57 pm. Thus, depending on the required resolution, relatively little may be gained by integrating over long times to collect "clean" spectra. For our work, a collection time of 1 second represents a two-order-of-magnitude speed increase over previous measurements with these structures [20].

Final issues include: (i) an Ar^+ laser represents a significant experimental cost. However, a 405-nm LED also excites the QDs and also gives good WGM spectra. (ii) Additional sources of error (probably quite significant ones) are certainly present in our experimental results, which appear to converge toward a detection limit of ~60 pm rather than the predicted values < 1pm. Temperature variations or any other quantifiable source of experimental error in the peak location can be added in quadrature to the resolution obtained from Eqs. (3) and (4).

#161306 - $15.00 USD Received 11 Jan 2012; revised 27 Feb 2012; accepted 4 Mar 2012; published 26 Mar 2012

Conclusions

A simple numerical relationship was obtained for quickly estimating the resolution and detection limits for WGM-based refractometric sensor devices, regardless of the measurement system and device platform. Although initially motivated by examining the resolution limits of fluorescent-type devices such as ring resonators, capillaries, and microspheres, the results apply to evanescently-coupled devices also. The numerical resolution models of Eqs. (3) and (4) are general and include the effect on the ultimate system resolution of the sampling for different but commonly-used peak shift measurement methods. While we stress that this work does not develop any novel signal processing methods, the results are fairly encouraging from the point of view of fluorescence WGM sensing, where a resolution of ~1 pm might be expected when the modes are non-overlapping Lorentzians. Collection times, too, can be much lower than previously thought possible for extracting meaningful wavelength shifts. The Fourier method, especially, can provide a good resolution, relative insensitivity to noise, easy software integration for live-time analysis, and a minimization of subjective modeling input. Further improvements might be possible, for example, by using least-squares frequency analysis to deal with non-uniform spectral sampling, or by incorporating waveform variations in addition to a pure shift.

Acknowledgments

We thank NSERC and CIPI for funding this research, and an anonymous "signal processing purist" for comments that led to an improvement of this manuscript.

#161306 - $15.00 USD Received 11 Jan 2012; revised 27 Feb 2012; accepted 4 Mar 2012; published 26 Mar 2012